# Advanced Transmission Raman Spectroscopy: A Promising Tool for Breast Disease Diagnosis

Nicholas Stone[1] and Pavel Matousek[2]

[1]Biophotonics Research Unit, Gloucestershire Royal Hospital, Gloucester, United Kingdom and [2]Central Laser Facility, Science and Technology Facilities Council, Rutherford Appleton Laboratory, Didcot, Oxfordshire, United Kingdom

## Abstract

**A novel approach to noninvasively probe the composition of endogenous materials concealed deeply within mammalian tissue is presented. The method relies upon transmission Raman spectroscopy and permits the detailed characterization of the chemical composition of the probed volume. The technique has been enhanced by the deployment of chemometric methods and the use of a dielectric optical element at the surface to force escaping photons back into the tissue and, thus, enhance the relatively weak signals from the deeper tissue and its components. This permitted reaching both the clinically relevant depth and sufficient sensitivity in phantoms for the noninvasive identification of the calcification types associated with benign or malignant breast disease. Both calcium hydroxyapatite and calcium oxalate monohydrate have been chemically identified from depths of up to 2.7 cm within a breast phantom made up of porcine tissues. The technique has shown significant potential for probing human breasts to provide complementary data in the early diagnosis of breast cancer.** [Cancer Res 2008;68(11):4424–30]

## Introduction

Mammography can detect small masses, areas of distortion, ill-defined densities, and microcalcifications not detectable by physical examination. However, contrast is dependent only on the morphology and density of the specimen, not the chemical constituency. This limitation means it gives no definitive criteria for classifying benign and malignant calcifications, and as such, only 10% to 25% of mammographically detected lesions are found to be malignant upon needle biopsy (1, 2). Calcification appearance on mammography is a feature of a proportion of breast cancers, and its occurrence does not correlate with either age or primary tumor size. It has been shown by Holme and colleagues (1993; ref. 3) that a significantly larger number of lymph nodes are involved in patients with tumors showing microcalcifications than those without. This suggests a biologically significant role for the deposition of calcium in microcalcifications that may relate to the process of tumor cell metastasis. As such, determining the relationship between microcalcifications and tumor cell metastasis is regarded as a high priority to aid the assessment of patients with cancers that show microcalcification on mammography.

Microcalcifications can be divided into two types of deposits: type I, which consist of calcium oxalate dihydrate (COD), and type II, which are composed of calcium phosphates, mainly calcium hydroxyapatite (HAP). The type of deposit has been correlated with disease (4). Calcium oxalate crystals are mainly found in benign ductal cysts and rarely found in carcinoma, whereas HAP deposits are found within proliferative lesions, which include carcinomas. At present, there is no reliable way to distinguish between these two types of calcification by mammography. However, the calcifications can be distinguished from their chemical makeup by using vibrational spectroscopy (IR spectroscopy or Raman spectroscopy). Although, to be truly effective *in vivo*, any technique should be able to be used transcutaneously, so as to enable a quick and simplistic diagnosis of breast lesions, thus minimizing the patient trauma, time delay, and high medical costs of biopsies. Here, we explore the possibility of the use of advanced near-IR transmission Raman spectroscopy to achieve this goal.

Raman spectroscopy uses the molecular-specific energy shifts in inelastically scattered light. The optimum wavelengths for Raman tissue work have been shown to be in the near-IR region of between 785 and 840 nm. This represents a compromise between minimizing interference from fluorescence, which usually swamps the weaker Raman signals, and working within the spectral region where highly sensitive charge coupled detectors (CCD) can be used to detect the low levels of Raman photons (5).

The use and sensitivity of Raman spectroscopy as an analytic technique capable of distinguishing between normal and malignant breast tissues (1, 6) and between different pathologic grades of breast and other epithelial tissues has already been established (7–13). Furthermore, it has recently been shown that Raman spectroscopy is capable of distinguishing between the two types of calcification in excised breast tissue with a high degree of accuracy (4). However, it is currently unclear whether the Raman technique can be applied to detect and distinguish microcalcifications *in vivo* and nondestructively.

**Advanced depth probing with Raman.** Previous work by ourselves and others has shown the potential for depth probing in biological tissues, by effectively suppressing the relative signal level from the surface and, thus, enhancing the relative signal level from the depth of interest (14–20). A number of approaches have been used, ranging from time gating of the collected signal (Kerr-gating) after a picosecond laser pulse, to spatially offsetting the point of collection from the point of illumination (SORS) and to transmission Raman spectroscopy, which has thus far achieved the deepest penetration depth into biological tissue. In this study, a novel step to significantly improve on the earlier transmission Raman approach was taken by use of a dielectric filter on the surface of the tissue to enhance the Raman-scattered signal obtained from deep within the tissue. The diffuse nature of photons propagating in tissue prevents focused delivery and collection of laser light to a

**Note:** Supplementary data for this article are available at Cancer Research Online (http://cancerres.aacrjournals.org/).

**Requests for reprints:** Nicholas Stone, Gloucestershire Hospitals NHS Foundation Trust/Cranfield University, Great Western Road, Gloucester, GL1 3NN, United Kingdom. Phone: 44-0-8454-225486; Fax: 44-0-8454-225485; E-mail: n.stone@medical-research-centre.com.



doi:10.1158/0008-5472.CAN-07-6557

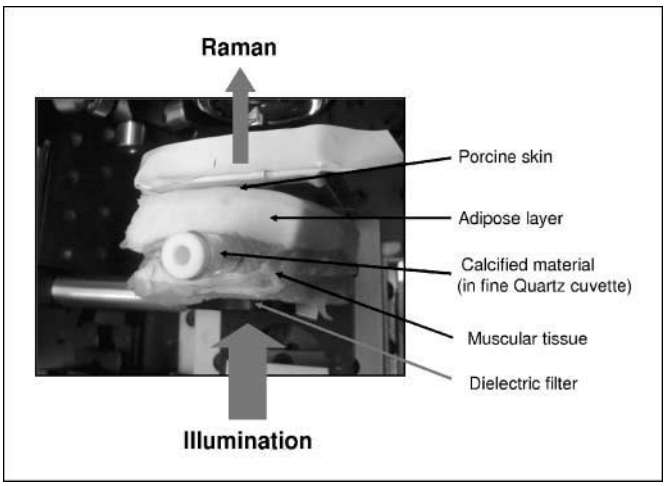


**Figure 1.** Photograph of 27 × 50 × 50 mm mixed porcine tissue slab (human breast phantom) with quartz vial containing calcified material inserted.

target zone. The effective coupling of laser radiation into deep layers of tissue and powders is also severely hindered by excessive photon loss occurring at the coupling sample-to-air interface caused by the high scattering nature of tissue. This effect can lead to the loss of the majority of laser radiation at the surface of the sample before it can reach the target layer as evident from an earlier work by Kubelka and Munk (21), Schrader and Bergmann (22), and Schrader and Moore (23). Here, we present a simple, practical method enabling dramatic enhancement of the level of laser radiation reaching the target layer and consequently the Raman signal itself, typically severalfold, using a dielectric interference element placed over the laser illumination region on tissue surface. The concept has been proposed earlier and shown with powder samples (24). Here, we show its applicability for the first time with biological tissue samples. Supplementary information is provided, outlining the experimental methods and apparatus used for this study.

## Materials and Methods

**Specimens.** A breast tissue phantom was constructed from porcine tissue, to include skin, adipose, and muscular tissues. Thicknesses of >20 mm were used in the transmission direction, and maximum lateral dimensions of >50 mm were used to minimize photon migration from the lateral edges. The size of the phantom can be considered as semi-infinite in optical terms, where the mean-free-path between scattering and absorption events will be of the order of 0.1 mm. With these dimensions, lateral photon escape is minimized. The threshold for potentially useful *in vivo* clinical measurements is >20 mm (25). The fresh porcine tissue was obtained from a local butcher and cut to the desired thickness. A small slit along one edge was cut into the phantom with a

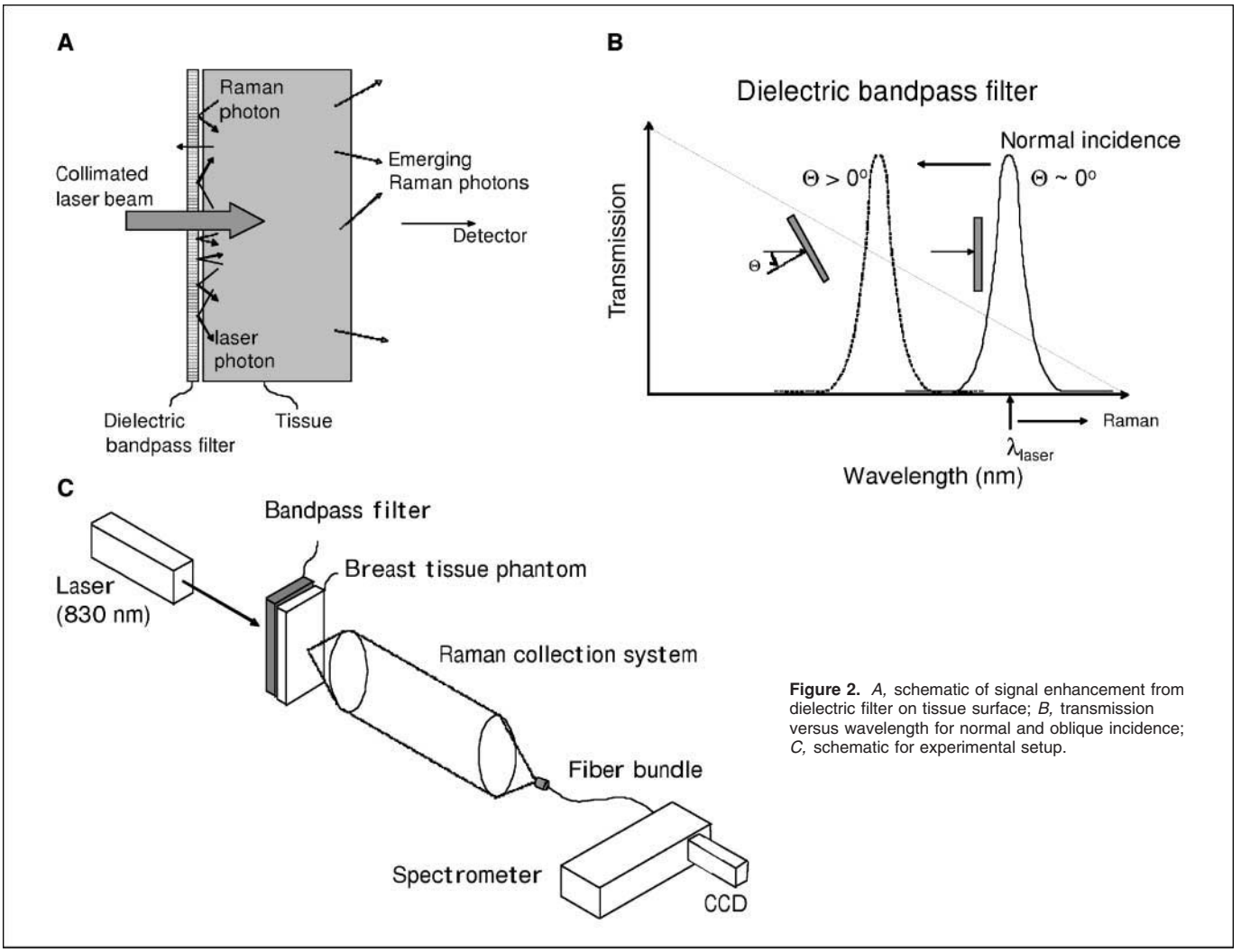


**Figure 2.** *A,* schematic of signal enhancement from dielectric filter on tissue surface; *B,* transmission versus wavelength for normal and oblique incidence; *C,* schematic for experimental setup.

scalpel to allow insertion of the calcified material into the center of the tissue (see Fig. 1). The samples were stored in a refrigerator and warmed to room temperature before use.

Polycrystalline standards were purchased (Clarkson Chromatography Products, Inc.) of "pure" HAP and calcium oxalate monohydrate (COM). These fine powders were evenly distributed within the cavity of a quartz vial (30 × 10 × 2 mm) with a 1.4-mm-thick cavity and with 300-μm UV-grade quartz windows. An assumption is made that in a first approximation, the geometry of the calcified material is less important than the volume of the material relative to the tissue volume probed. The material of composition of type II calcifications, COD, is difficult to manufacture due to its inherent thermodynamic instability. In this study, we used COM as a substance with similar properties to COD but available for purchase (Sigma-Aldridge).

**Apparatus.** The Raman spectra in this work were obtained using a modified SORS set up developed for noninvasive spectroscopy of bones described earlier (17). The probe beam was generated using a temperature-stabilized diode laser for Raman spectroscopy and operating at 830 nm (Process Instruments, Inc.; PI-ECL-830-300-FS). The laser power was ~250 mW at the sample, and the laser spot diameter before the sample was ~4 mm (power density, 19 $mW.mm^{-2}$). This exceeds the maximum permissible exposure (MPE) as defined by EN 60825-1:2007 for 830-nm continuous wave illumination (MPE is 3.639 $mW.mm^{-2}$ and would require only 45.73 mW to be used in 4-mm spot). However, no damage to the tissue was observed and heat dissipation is significantly enhanced in live perfused tissue. The beam was spectrally purified by removing any residual amplified spontaneous emission components from its spectrum using three 830-nm bandpass filters (Semrock).

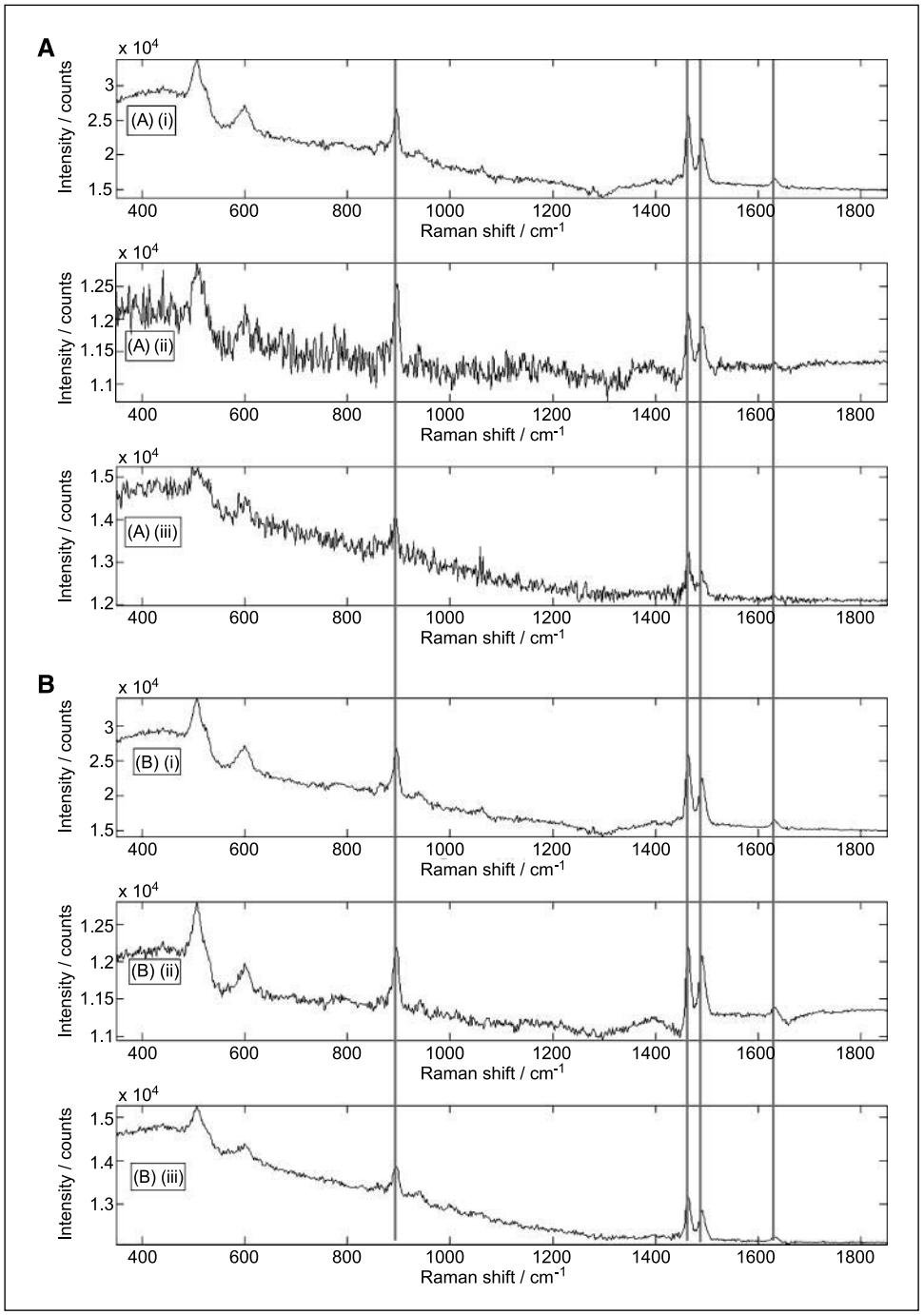


**Figure 3.** *A,* difference spectra from tissue with and without type I material (COM) present for three breast phantoms: (*i*) 17 mm mixed tissue, (*ii*) 27 mm muscle only, and (*iii*) 26 mm mixed tissue. *B,* difference spectra after PC noise reduction for tissue with and without type I material (COM) present for three breast phantoms: (*i*) 17 mm mixed tissue, (ii) 27 mm muscle only, and (*iii*) 26 mm mixed tissue. Acquisition times were 5 s with 10 accumulations for all spectra shown. *Vertical lines,* COM peaks.

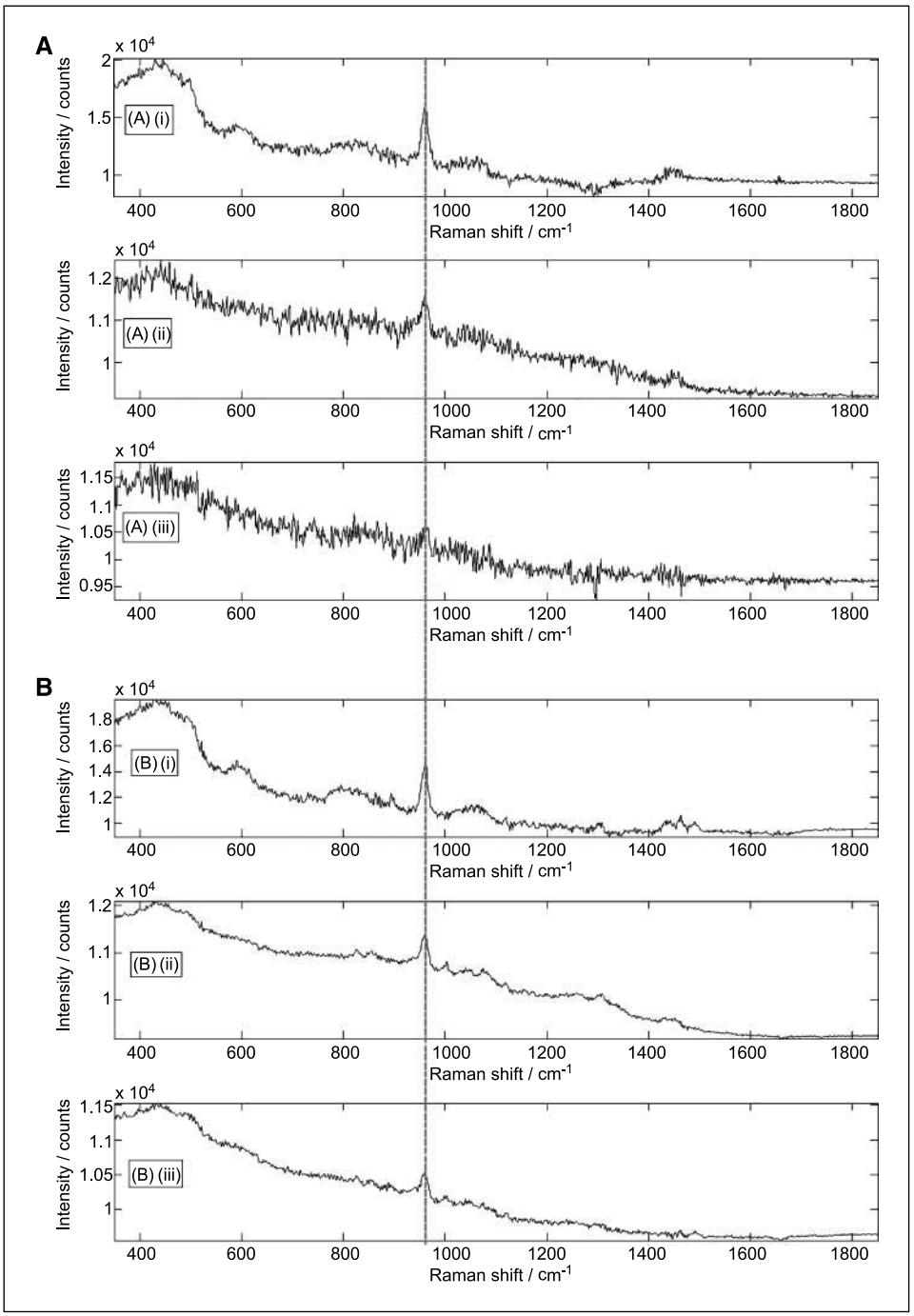


**Figure 4.** *A,* difference spectra from tissue with and without type II material (HAP) present for three breast phantoms: (*i*) 17 mm mixed tissue, (*ii*) 27 mm muscle only, and (*iii*) 26 mm mixed tissue; *B,* difference spectra after PC noise reduction for tissue with and without type II material (HAP) present for three breast phantoms: (*i*) 17 mm mixed tissue, (*ii*) 27 mm muscle only, and (*iii*) 26 mm mixed tissue. Acquisition times were 5 s with 10 accumulations for all spectra shown. *Vertical line,* HAP peak.

An enhancement of Raman signal is achieved in a simple passive manner by placing a multilayer dielectric element into the laser beam in the proximity of the probed turbid sample. The photon loss is prevented using the well-known angular properties of the multilayer dielectric bandpass filter, which, in general, exhibits a strong dependence on photon incidence angle with the spectral transmission window shifting to the blue part of the spectrum upon the increase of the photon deviation away from normal incidence (26). Thus, such photons are reflected instead of transmitted through a filter with such properties. If the filter is designed to transmit collimated laser light at normal incidence, then this element can be used to act as a unidirectional mirror transmitting a semicollimated laser beam affecting on it at normal incidence at one side, whereas at the other side, reflecting the majority of laser photons emerging from the sample in random directions back into the medium (see Fig. 2*A–B*).

A 25-mm dielectric bandpass filter centered at 830 nm with a bandwidth of 3.2 nm (Semrock LL01-830-25; MaxLine Laser-line Filter) was placed over the laser beam deposition area on the sample. The filter has a transmission at 830 nm of >90%. Raman spectra were measured of the transmission through the tissue phantom with and without the type I and type II calcified material present for each phantom. Phantom composition and depths were varied to evaluate limitations of the technique, and the relative concentration of the calcified material was reduced to approximate physiologic levels in a final experiment, to show proof-of-principle.

The transmitted Raman light was collected using a standard 50-mm diameter fused silica lens with a focal length of 60 mm. No antireflection coating was used. The scattered light was collimated and passed through a 50-mm diameter holographic notch filter (830 nm; Kaiser Optical Systems, Inc.) to suppress the elastically scattered component of light. The second

lens, identical to the first, was then used to image, with magnification 1:1, the sample interaction zone onto the front face of a fiber bundle (see below). The laser incident spot was positioned in such a way so that it coincided with the center of the fiber probe axis projected through the imaging system on the sample (see Fig. 2*C*).

The fiber bundle collecting the Raman light consisted of 22 active fibers made of silica with a core diameter of 220 μm, a doped silica cladding diameter of 240 μm, and a polyimide coating of 265 μm diameter. The fiber numerical aperture was 0.37. The bundle was custom made by CeramOptec Industries, Inc. The Raman scattered light was propagated through the fiber bundle of length ~2 m to the end with the fibers mounted in a linear array, which was oriented vertically and placed in the input image plane of a Kaiser Optical Technologies Holospec 1.8i NIR spectrograph. Raman spectra were collected using a NIR back-illuminated deep-depletion TE-cooled (−80°C) CCD camera (Andor Technology; DU420A-BR-DD; 1,024 × 256 pixels) by binning the entire chip vertically. Acquisition times were 5 s with 10 accumulations for each measurement. The Raman spectra were not corrected for the variation of detection system sensitivity across the spectral range.

## Results

The spectra collected from the breast phantom (Fig. 1) using the advanced transmission Raman apparatus were imported into Matlab 7 to enable simple numerical manipulation. First, the recovery of the spectra of specific calcification material from up to 27 mm of porcine tissue was achieved by calculation of difference spectra between the phantom with and the phantom without calcifications of each type. Thicknesses up to 26 mm of mixed skin/fat/muscle were used or 27 mm of pure muscle tissue. It was noted that in this configuration, the dielectric filter enhanced the signal level by ~1.5 times.

Figures 3*A* and 4*A* show the potential for discrimination between the calcified material found buried within the tissues. The peaks for COM at 898, 1,462, 1,490, and 1,634 $cm^{-1}$ and HAP at 962 $cm^{-1}$ are clearly visible for all these measurements. The dashed vertical lines on the figures show the COM peaks and the dotted vertical line the HAP peak.

Further data analysis involving high spectral variance principal component (PC) reconstruction of the spectra enabled significant random noise reduction in the signal and, hence, significant enhancement of the calcification signal to noise (see Figs. 3*B* and 4*B*). This actually indicates the possibility of recovering signals from even greater depths than measured here, even without further technical modifications of the apparatus.

The second part of this study involved the reduction of the calcifications to levels likely to be found in typical physiologic conditions in the breast. In our previous article (20), we estimated that in terms of sensitivity to the clinically relevant concentrations of calcifications, we were around an order of magnitude below the clinically relevant levels. The percentage volume density ratios from the literature were approximated to around 0.14% for benign and 0.05% for malignant. In this study we used 1.25% and finally 0.125% HAP and were still able to recover a signal to provide identification of calcification type. Figure 5 shows the recovered signal achieved for 0.125% (relative volume) of HAP buried within 20 mm of porcine tissue.

The next possibility is for an automated prediction of calcification type. A spectral data set constructed from spectra measured from tissue alone, tissue with HAP, and tissue with COM has been used to construct a simple mean-centered principal component model. The first 10 loads are shown in Fig. 6*A*. They show spectrally useful information in the first eight components from this small data set. These loads represent the first 99% of the total spectral variance of the data. Figure 6*B* shows a scores plot for the two most significant principal components for maximal separation of the three groups, calculated using ANOVA (Student's *t* test extended to greater than two groups; ref. 27). This shows that even with simple unsupervised classification, it may be possible to use a spectral classification model to predict calcification type in real-time.

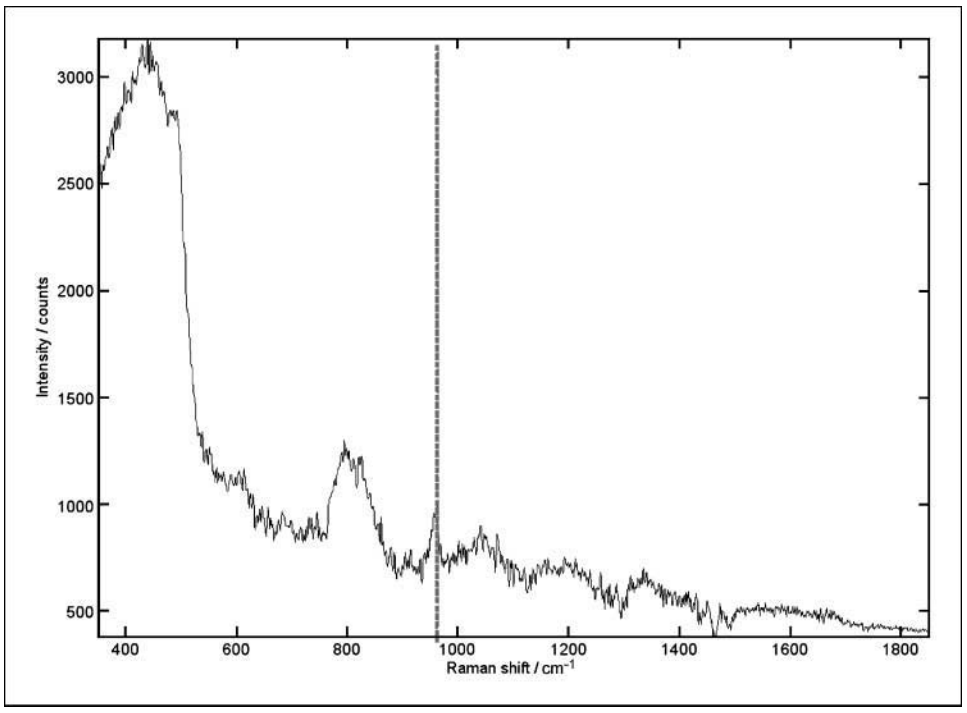


**Figure 5.** The recovered signal achieved for 0.125% (relative volume) of HAP buried within 20 mm of porcine tissue. The 962 $cm^{-1}$ peak is still clearly recognizable. Acquisition times were 5 s with 10 accumulations. *Vertical line,* HAP peak.

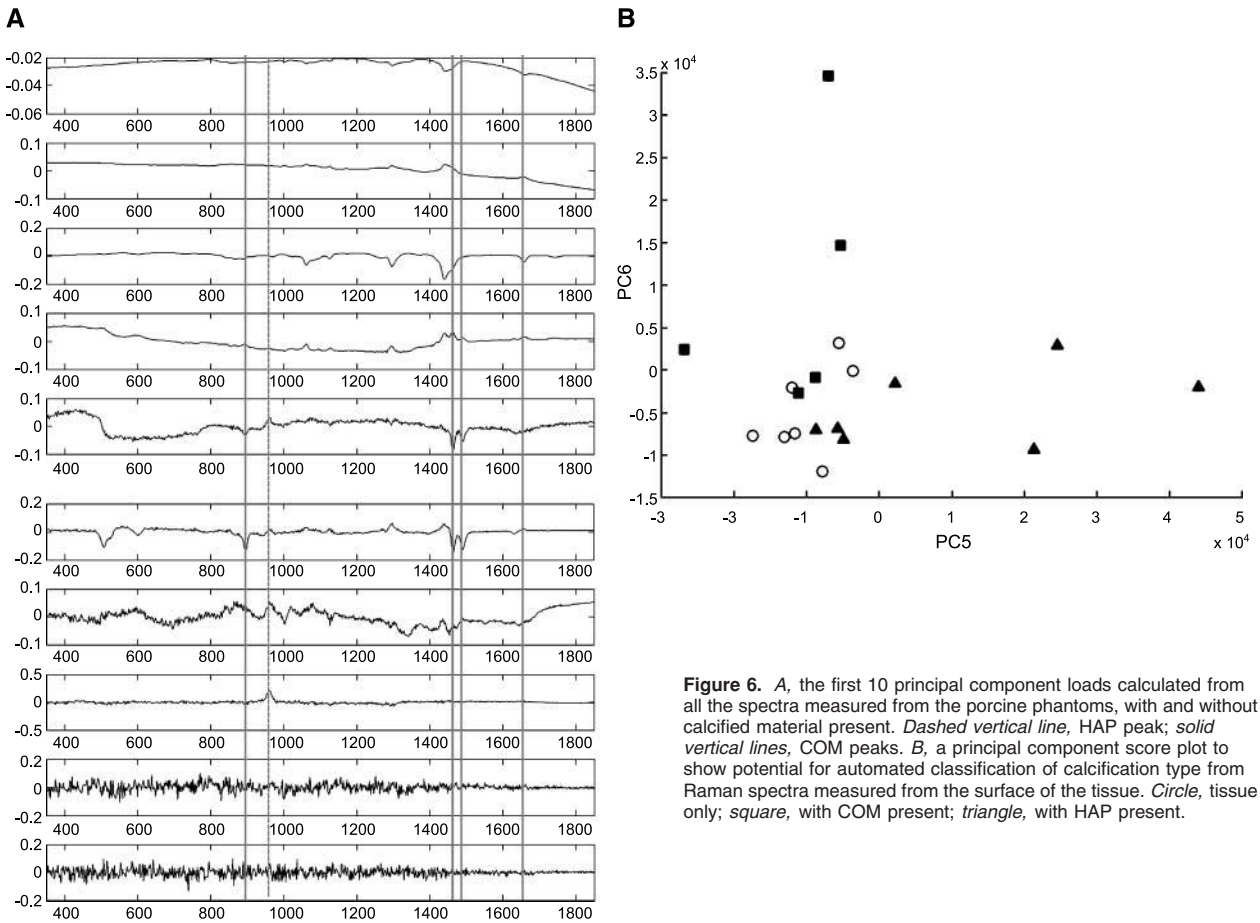


**Figure 6.** *A,* the first 10 principal component loads calculated from all the spectra measured from the porcine phantoms, with and without calcified material present. *Dashed vertical line,* HAP peak; *solid vertical lines,* COM peaks. *B,* a principal component score plot to show potential for automated classification of calcification type from Raman spectra measured from the surface of the tissue. *Circle,* tissue only; *square,* with COM present; *triangle,* with HAP present.

## Discussion

We discussed in a previous article (20) that it would be theoretically possible to improve on the 16-mm depth probing of calcified material in chicken breast (which was previously achieved without the advance of the dielectric filter at the surface to enhance the deep Raman signal) with a number of possible developments. This improvement coupled to more advanced data processing has lead to significant improvements in signals from greater depths. Furthermore, the use of mammalian tissues in the phantom, covering the gross tissue composition likely in the human breast, and the reduction in calcification volume density has made this proof-of-principle much closer to human *in vivo* measurements. Note the signal contributions using transmission Raman come from relative amounts of the constituents, so the layering structure does not have to be precisely the same provided the constituents are present in similar amounts.

The dielectric filter was observed to improve the signal by a small margin of around 50% within the porcine tissue phantom. The degree of enhancement would be likely to be dependent on the optical properties of the medium, such as absorption and scattering coefficients. In heavily pigmented tissue, this is likely to lead to a lower signal improvement attributable to the filter. However, as the quality of the signal depends on many factors, of which the filter enhancement plays a minor role, the overall reduction of signal-to-noise in pigmented tissue due to a reduction in this enhancement would not be expected to be dramatic.

Further improvements in the penetration depth and technique sensitivity can be achieved using higher-power defocused laser beams delivered into larger areas permitted by the transmission Raman geometry and by further optimizing the collection system to collect Raman signals effectively from larger areas. The latter can be achieved using wider spectrograph slits enabling the coupling of a larger number of fibers into the detection system while maintaining the spectral resolution. This can be accomplished, for example, by using larger dispersion gratings in the spectrograph and a consequently narrower spectral region centered only on the spectral region of interest where major differences between different calcifications are present. This could provide a signal enhancement of a factor of 10.

If the power density of laser illumination was kept constant, we can raise the overall power to the sample to 1.49 W in 10-mm spot (19 $mW.mm^{-2}$), or ~6 W in a 20-mm spot. However, this power density is substantially lower than that used in other studies *in vivo*, such as that used in work by Enejder and colleagues (28), where illumination intensity of 300 $mW.mm^{-2}$ was used safely. We may be able to increase our power even further, although further study is required to understand the potential problems of volume heat dissipation at these intensities. From the above, we estimate that it should be technically feasible to increase the

laser power by a factor of at least 24 [to 6 W in 20-mm spot (still 19 $mW.mm^{-2}$)].

We are on the threshold of clinically relevant sensitivity and penetration depth; however, any further improvements would be highly desirable for real world clinical delivery. Overall, the above improvements should result in an enhancement factor of 240, projecting into a signal-to-noise ratio enhancement of the Raman spectra of ~15 (20). This should dramatically improve the prospects of the deployment of the technique for *in vivo* screening, which will be a focus of our next research.

## Conclusions

We have shown for the first time the facility of advanced transmission Raman spectroscopy to detect and identify the chemical composition of calcified material within a clinically relevant depth of 27 mm within mammalian tissue. This is the highest depth reported thus far and within the clinically relevant range of potential application in diagnosis of human breast cancer *in vivo*.

A further test was made to establish whether clinically relevant calcification volumes could be measured with this technique. The identification of HAP at 20 mm with an approximate volume ratio of around $1.25 \times 10^{-3}$ was achieved with this technique. This is within the calculated clinical range for effective calcification concentrations found in sampling volumes.

These results pave the way for the potential development of new noninvasive diagnostic techniques for calcification-associated breast disease applicable in conjunction with existing mammography or ultrasound techniques to enhance their diagnostic potential.

## Disclosure of Potential Conflicts of Interest

P. Matousek and N. Stone: ownership interest, Patent JRP/P85898GB00 on SORS for breast cancer.

## Acknowledgments

Received 12/7/2007; revised 3/3/2008; accepted 3/28/2008.

**Grant support:** Dr. Darren Andrews, Professor Anthony Parker and Dr. Mike Dunne of Council for the Central Laboratory of the Research Councils, and the financial contribution of the Central Laboratory Innovation and Knowledge Transfer Limited, National Endowment for Science, Technology and the Arts, and Rainbow Seed Fund enabling this study. Professor Keith Rogers and Rebecca Baker of Cranfield University have strongly supported this study as part of the ongoing program investigating the effect of breast calcifications on carcinogenesis processes and their potential to enhance understanding and diagnosis. NIH Career Scientist Fellowship supported by the UK Department of Health (N. Stone).

The costs of publication of this article were defrayed in part by the payment of page charges. This article must therefore be hereby marked *advertisement* in accordance with 18 U.S.C. Section 1734 solely to indicate this fact.

## References

1. Haka AS, Shafer-Peltier KE, Fitzmaurice M, Crowe J, Dasari RR, Feld MS. Diagnosing breast cancer by using Raman spectroscopy. Proc Natl Acad Sci U S A. 2005;102:12371–6.
2. Evans AJ, Wilson AR, Burrell HC, Ellis IO, Pinder SE, Mammographic features of ductal carcinoma *in situ* (DCIS) present on previous mammography. Clin Radiol 1999;54:644–6.
3. Holme TC, Reis MM, Thompson A, et al., Is mammographic microcalcification of biological significance? Surg Oncol 1993;19:250–3.
4. Haka AS, Shafer-Peltier KE, Fitzmaurice M, Crowe J, Dasari RR, Feld MS. Identifying differences in microcalcifications in benign and malignant breast lesions by probing differences in their chemical composition using Raman spectroscopy. Cancer Res 2002;62:5375–80.
5. Stone N. Raman Spectroscopy of Biological Tissue for Application in Optical Diagnosis of Malignancy. PhD thesis, Cranfield University UK, (2001).
6. Dukor RK, Liebman MN, Johnson BL. A new, non-destructive method for analysis of clinical samples with FT-IR microspectroscopy. Breast cancer tissue as an example. Cell Mol Biol (Noisy-le-grand) 1998;44:211–7.
7. Robichaux-Viehoever A, Kanter E, Shappell H, Billheimer D, Jones III H, Mahadevan-Jansen A, Characterization of Raman spectra measured *in vivo* for the detection of cervical dysplasia. Appl Spectrosc 2007;61:986–93.
8. Stone N, Stavroulaki P, Kendall C, Birchall M, Barr H. Raman spectroscopy for early detection of laryngeal malignancy: preliminary Results. Laryngoscope 2000;110:1756–63.
9. Stone N, Kendall C, Shepherd N, Crow P, Barr H, Near-infrared Raman spectroscopy for the classification of epithelial pre-cancers and cancers., Journal of Raman Spectroscopy 2002;33:564–73.
10. Crow P, Kendall C, Wright M, Persad R, Ritchie A, Stone N. The use of Raman spectroscopy to distinguish between normal tissue, carcinoma *in situ* and TCC within the bladder. Br J Urol 2002;90:71.
11. Kendall C, Stone N, Shepherd N, et al. Raman spectroscopy a potential tool for the objective identification and classification of neoplasia in Barrett's oesophagus. J Pathol 2003;200:602–9.
12. Crow P, Stone N, Kendall CA, et al. The use of Raman spectroscopy to identify and grade prostatatic adenocarcinoma *in vitro*. Br J Cancer 2003;89:106–9.
13. Shetty G, Kendall C, Shepherd N, Stone N, Barr H. Raman spectroscopy: elucidation of biochemical changes in carcinogenesis of oesophagus. Br J Cancer 2006;94:1460–4.
14. Hart Prieto MC, Matousek P, Towrie M, et al. The use of picosecond Kerr gated Raman spectroscopy to suppress signals from both surface and deep layers in bladder and prostate tissue. J Biomed Opt 2005;10:044006.
15. Morris MD, Matousek P, Towrie M, Parker AW, Goodship AE, Draper ERC. Kerr-gated time-resolved Raman spectroscopy of equine cortical bone tissue. J Biomed Opt 2005;10:014014.
16. Baker R, Matousek P, Ronayne K, Parker AW, Rogers K, Stone N, Depth profiling of calcifications in breast tissue using picosecond Kerr-gated Raman spectroscopy. Analyst 2007;132:48–53.
17. Matousek P, Clark IP, Draper ERC, et al. Subsurface probing in diffusely scattering media using spatially offset Raman spectroscopy. Appl Spectrosc 2005;59:393–400.
18. Stone N, Baker R, Rogers K, Parker AW, Matousek P. Future possibilities in the diagnosis of breast cancer by subsurface probing of calcifications with spatially offset Raman spectroscopy (SORS). Analyst 2007; 132:899–905.
19. Schulmerich MV, Dooley KA, Morris MD, Vanasse TM, Goldstein SA. Transcutaneous fiber optic Raman spectroscopy of bone using annular illumination and a circular array of collection fibers. Indicators of bone quality. J Biomed Opt 2006;11:060502.
20. Matousek P, Stone N. Prospects for the Diagnosis of Breast Cancer by Non-Invasive Probing of Calcifications using Transmission Raman Spectroscopy. J Biomed Opt 2007;12:024008.
21. Kubelka P, Munk F, Ein Beitrag Zur Optik der Farbanstriche. Zeitschrift fur technische Physik 1931;12:593–601.
22. Schrader B, Bergmann G. Die Intensitat des Ramanspektrums polykristalliner substanzen I. Strahlungsbilanz von Substanz und Probenanordnung. Z Anal Chem Fresenius 1967;225:230–47.
23. Schrader B, Moore DS. Laser-based molecular spectroscopy for chemical analysis-Raman scattering processes. Pure Appl Chem 1997;69:1451–68.
24. Matousek P, Raman Signal Enhancement in Deep Spectroscopy of Turbid Media. Appl Spectrosc 2007;61:845–54.
25. Sardanelli F, Zandrino F, Imperiale A, Bonaldo E, Quartini MG, Cogorno N. Radiology 2000;217:576–80.
26. Born M, Wolf E. 'Principles of Optics.' 7th ed. Cambridge University Press.
27. Fisher LD, Van Belle G. Analysis of Variance. In: Biostatistics: A Methodology for the Health Sciences. John Wiley & Sons; 1993 p. 418–25.
28. Enejder AMK, Scecina TJ, Oh J, et al., Raman spectroscopy for noninvasive glucose measurements. J Biomed Opt 2005;10:031114.

# Advanced Transmission Raman Spectroscopy: A Promising Tool for Breast Disease Diagnosis

Nicholas Stone and Pavel Matousek

*Cancer Res* 2008;68:4424-4430.